ACS OMEGA

http://pubs.acs.org/journal/acsodf

Article

Superhydrophobic Electrodeposited Copper Surface for Robust Condensation Heat Transfer

Junghyun Park, Donghyun Kim, Hyunsik Kim, Woon Ik Park, Junghoon Lee,* and Wonsub Chung*

Cite This: *ACS Omega* 2022, 7, 19021−19029

Read Online

ACCESS | Metrics & More | Article Recommendations

ABSTRACT: Superhydrophobic surfaces have great potential for various applications owing to their superior dewetting and mobility of water droplets. However, the physical robustness of nano/microscale rough surface structures supporting superhydrophobicity is critical in real applications. In this study, to create a superhydrophobic surface on copper, we employed copper electrodeposition to create a nano/microscale rough surface structure as an alternative to the nanoneedle CuO structure. The rough electrodeposited copper surface with a thin Teflon coating shows superhydrophobicity. The enhancement of dewetting and mobility of water droplets on copper surfaces by electrodeposition and hydrophobization significantly improved the condensation heat transfer by up to approximately 78% compared to that of copper substrates. Moreover, the nano/microscale rough surface structure of the electrodeposited copper surface exhibits better tolerance to physical rubbing, which destroys the nanoneedle-structured CuO surface. Therefore, the condensation heat transfer of the superhydrophobic electrodeposited copper surface decreased by only less than 10%, while that of the nanoneedle-structured CuO surface decreased by approximately 40%. This suggests that an electrodeposited copper surface can lead to the stable performance of superhydrophobicity for real applications.

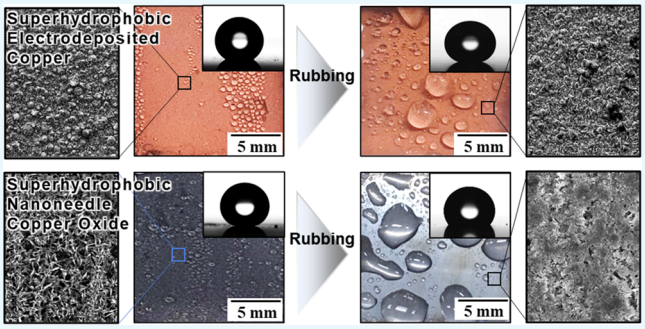

1. INTRODUCTION

Condensation is a ubiquitous phenomenon in the natural environment and is applied to various engineering systems, such as water harvesting, energy conversion, and heat management systems.[1−3] In particular, the condensation heat transfer caused by the release of latent heat to the surface of the condenser at a lower temperature than that of vapor, where the phase change from vapor to liquid occurs, is significant in heat-exchange systems. The condensed liquid water forms a film or droplet depending on the wettability of the cold surface. Condensed water forms a film on a highly wettable (hydrophilic) surface, while water droplets are formed on a dewettable (hydrophobic) surface.[4−7] Condensed water easily spreads to form a liquid film on the hydrophilic cold surface, which can act as a thermal barrier to inhibit the heat transfer between the ambient and cold solid surfaces.[8,9] Moreover, the unremovable water film causes local accumulation of contaminants and corrosion, which degrades heat transfer. In contrast, condensed water forms droplets on the hydrophobic surface so that the dewetted cold solid surface remains heat-transferred from the ambient.[10,11] In addition, because the contact area of a water droplet on a hydrophobic surface depends on the surface physical morphology, the mobility of water droplets on the surface can be enhanced.[12,13] Therefore, it is possible to remove condensed water droplets by gravital sliding or rolling along the surface, thereby exposing the dewetted cold solid surface to ambient conditions for continuous condensation.[14,15] Such effects enable hydrophobic surfaces to show a more enhanced condensation heat transfer than that of hydrophilic water-wettable surfaces. Therefore, the hydrophobization treatments of metallic materials can enhance the efficiency of heat exchangers, water harvesting and desalination, environmental control, and power generation.[16]

Copper and its alloys are among the most promising metallic materials in applications related to heat transfer because of their high thermal conductivity, ductility, and weldability.[17,18] Therefore, surface treatment and hydrophobization techniques that enhance condensation heat transfer have significant potential for various applications of copper. In addition, various strategies realizing hydrophobicity on copper surfaces have been widely explored because the dewetting surface provides anticontamination and anticorrosion.[19,20] A coating with low-surface energy materials and control of the surface morphology of copper are required to create a super-

Received: April 22, 2022
Accepted: May 16, 2022
Published: May 27, 2022

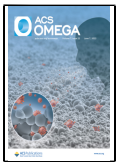

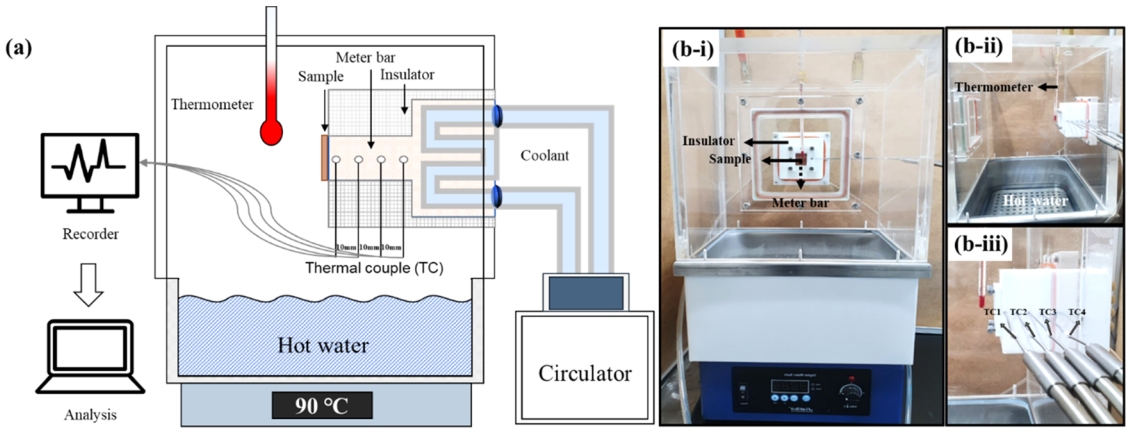

Figure 1. Test setup for condensation heat transfer: (a) schematic diagram and (b) photo images ((i) front view, (ii) side view, and (iii) side view of the meter bar with four thermocouples).

hydrophobic surface on copper. Thin layers of fluorocarbon materials (for example, Teflon, FDTS, and calcium stearate), which have a negligible effect on the surface morphology, are used to reduce the surface energy of copper.[21−23] According to the Cassie−Baxter rendering, sharp micro/nanoscale surface morphologies were created on copper for extremely high contact angles and mobility of water droplets.[24,25] Various techniques, including anodizing, chemical etching, thermal oxidation, and photolithography, have been applied to build nano- and microscale porous surface structures supporting superhydrophobicity.[26−28] In particular, a sharp nanoneedle CuO formed by simple chemical and thermal treatments has been widely applied to realize superhydrophobicity and enhance condensation heat transfer of copper and its alloys.[29,30] However, the nanoneedle CuO structure weakly adheres to copper and is brittle; thus, the surface structure is easily destroyed by slight physical damage, such as smooth rubbing with a finger. Therefore, the nanoneedle-structured CuO surface is unsuitable for real applications, such as condensation heat transfer, where long-term operation and maintenance are critical. For better durability, multistep electrodeposition of copper or electrodeposition in ionic liquids is introduced to create the superhydrophobic surface, but the fabrication processes are not suitable for practical applications with scalability.[31−33]

In this study, we employed a single-step electrodeposition of copper to create a nano/microsharp morphology on a copper substrate (CS) for the fabrication of durable superhydrophobic surfaces with enhanced condensation heat transfer. Copper is one of the most widely used metals for electrodeposition in practical fields. The physical morphology of the copper substrate can be controlled by a simple modification of processing parameters, such as the chemical composition of the electrolyte, current density, temperature, agitation, and additive. We adopted an electrodeposition condition to create a rough surface morphology of the copper layer, which was subsequently hydrophobized with a thin layer of poly(tetrafluoroethylene). Such a rough copper surface structure is expected to show better tolerance against physical damage than that of the nanoneedle CuO surface. In addition, the hydrophobized copper layer formed by electrodeposition had a lower thermal resistance than that of the nanoneedle CuO surface. The condensation heat transfer of the fabricated hydrophobic rough copper surface was evaluated and compared with that of the nanoneedle CuO surface. Moreover, we tested its tolerance against physical damage to maintain stable condensation heat transfer.

2. EXPERIMENTAL METHODS

A polished pure copper plate (more than 99.9%, thickness: 0.45 mm) cut into 40 mm × 25 mm pieces were used as the substrate for copper electrodeposition. The specimens were cleaned in ethanol with ultrasonication for 5 min and then rinsed with deionized (DI) water. The substrate was degreased in a 15 wt % sodium hydroxide (NaOH) solution for 1 min and then activated in 15 wt % hydrochloric acid (HCl) solution for 15 s. Copper was electrodeposited in an aqueous solution with 0.25 M copper sulfate pentahydrate ($CuSO_4 \cdot 5H_2O$), 0.5 M sulfuric acid (H_2SO_4), and 2.5 mM poly(ethylene glycol) (PEG, average molar weight 400) at 50 mA/cm^2 for 10, 20, and 30 min. The electrolyte was agitated with a stirring bar and maintained at 25 °C. The electrodeposited sample was cleaned with ethanol and dried with compressed air. The copper specimen activated in 0.08 M nitric acid was immersed in a 2.5 M NaOH + 0.13 M $(NH_4)_2S_2O_8$ solution at 60 °C for 40 min to create the nanoneedle CuO for comparison. After cleaning the surface with distilled water and ethanol, the specimen was heat-treated in an electric box furnace at 180 °C for 2 h. A thin layer of Teflon was coated with 0.2 wt % Teflon solution (a mixture of Teflon AF1600 powder (DuPont) and perfluorocompound (FC-40) to realize hydrophobicity on the copper surface).[34,35] A Teflon solution (20 μL/cm^2) was dropped on the copper surface, and the solvent was evaporated at 110 °C for 10 min; the Teflon film was baked at 250 °C for 15 min.

The surface morphology and topography were observed using field emission scanning electron microscopy (FE-SEM, Mira 3 LMH, Tescan) and atomic force microscopy (AFM, XE-100, Park Systems). The static contact angle and contact angle hysteresis were measured using a goniometer system (SmartDrop, Femtobiomed) at room temperature with a 5 μL water droplet. We fabricated a test setup to evaluate condensation heat transfer (Figure 1). Hot and humid conditions were formed using an acrylic box on an electric water bath. In addition, a copper meter bar (25 mm × 25 mm × 50 mm, more than 99.9%) cooled with circulating liquid was inserted through the acrylic box. The copper meter bar was covered with a Teflon insulator, and four T-type thermocouples were placed from the top surface at the centerline of the meter bar with a spacing of 10 mm. The sample was attached

https://doi.org/10.1021/acsomega.2c02522
ACS Omega 2022, 7, 19021−19029

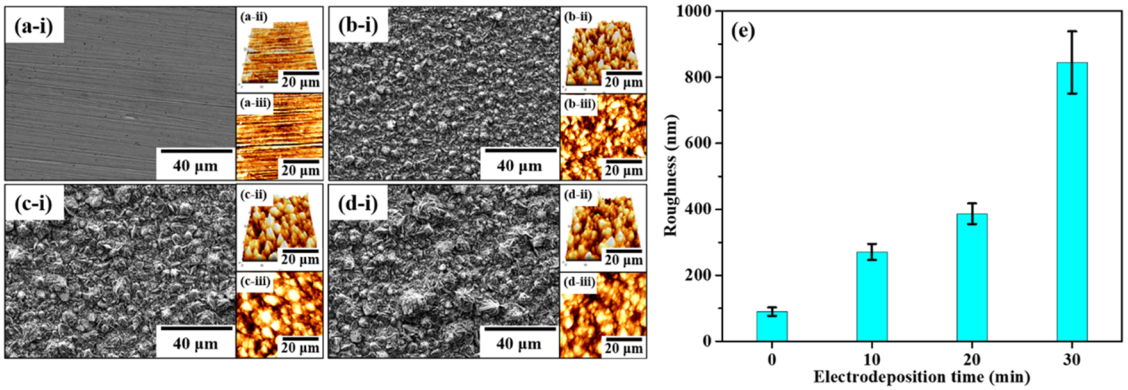

Figure 2. Surface morphology of (a) copper substrate and electrodeposited copper surface for (b) 10, (c) 20, and (d) 30 min. (i) SEM and AFM images from (ii) perspective view and (iii) top view. (e) Averaged roughness from AFM images.

to the top surface of the copper meter bar using thermal grease. The surface temperature of the sample was controlled by varying the temperature of the circulating coolant. The condensation heat transfer on the sample surface was estimated from the heat flux calculated from the temperature gradient in the meter bar and the thermal conductivity of the meter bar. The sample surface was intentionally damaged to test the tolerance to mechanical damage by a rubbing test (DIN EN ISO 11640). We used a rubber eraser as a counterpart of the rubbing test. The rubbing load, speed, linear distance, and total distance are 0.98 N, 20 cycle/min, and 0.5 and 20 cm, respectively.

3. RESULTS AND DISCUSSION

3.1. Fabrication of the Superhydrophobic Copper-Electrodeposited Surface. The wettability of a hydrophobic surface depends on the roughness with respect to Cassie–Baxter rendering.[36,37] The morphology and roughness of the sample surfaces with copper electrodeposition and the Teflon coating were characterized using SEM and AFM (Figure 2). The copper substrate (CS) had linear grooves formed by mechanical polishing. In addition, the Teflon coating used in this study only has a thickness of a few nanometers, so the hydrophobizing coating does not significantly affect the surface morphology.[38,39] In this study, we used a low-concentration electrolyte for copper electrodeposition and PEG as an additive, causing film growth in the preferred orientation of copper crystals.[27,40,41] Thus, randomly rough copper surface structures (Figure 2a–d) are created by electrodeposition, and the rough structure grows with an increase in electrodeposition time. The formation and growth of randomly rough surface structures contributed to the increase in surface roughness. The average roughness (R_a) increased from 90 ± 13 nm (for the copper substrate, CS) to 271 ± 25 nm after 10 min of electrodeposition (ED10), which further increased to 387 ± 31 and 845 ± 94 nm by copper electrodeposition for 20 min (ED20) and 30 min (ED30), respectively.

According to the Cassie–Baxter state, roughness is critical for improving the dewetting of hydrophobic surfaces formed by the Teflon coating with stability under hot and humid conditions.[42,43] Therefore, the Teflon coating on electrodeposited copper surfaces with different average roughness values results in varying wettability and mobility of water droplets. The apparent contact angle and contact angle hysteresis (advancing contact angle–receding contact angle) were measured to estimate the wettability and mobility of water droplets, respectively (Figure 3). In addition, water droplets mixed with a blue dye on the sample are shown in

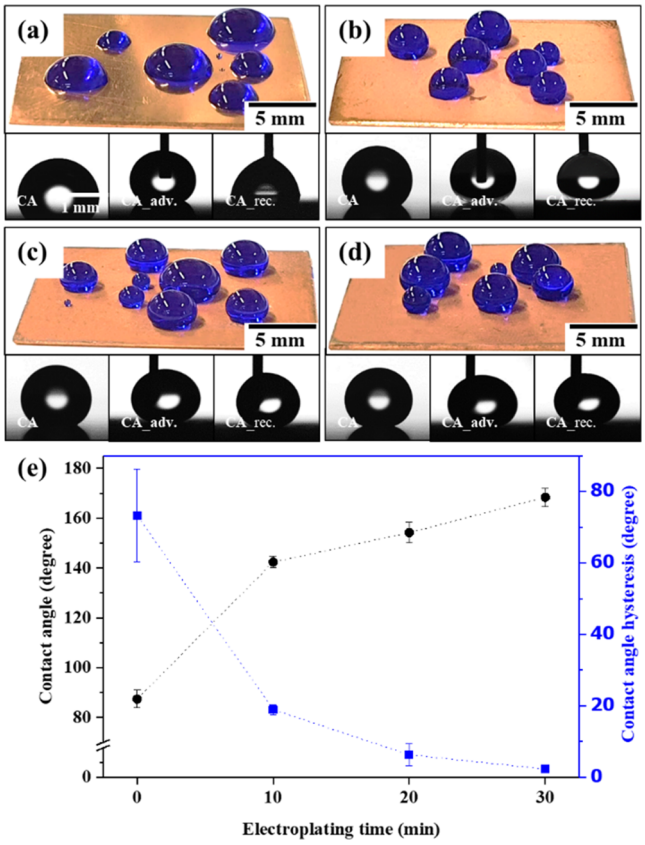

Figure 3. Image of water droplets on (a) copper substrate and hydrophobic copper surface electrodeposited for (b) 10 (ED10), (c) 20 (ED20), and (d) 30 (ED30) min. CA, CA_adv, and CA_rec indicate the static contact angle, advancing contact angle, and receding contact angle, respectively. (e) Averaged static contact angle and contact angle hysteresis.

Figure 3. The apparent contact angle and contact angle hysteresis of the water droplet on the copper substrate were 87.4 ± 3.5 and 73.3 ± 12.9°, respectively. The copper electrodeposition creating a randomly rough surface structure reduces the contact area of the water droplet on the solid surface, which significantly increases the contact angle with an increase in the surface roughness, such as 142.4 ± 2.3, 154.2 ±

https://doi.org/10.1021/acsomega.2c02522
ACS Omega 2022, 7, 19021–19029

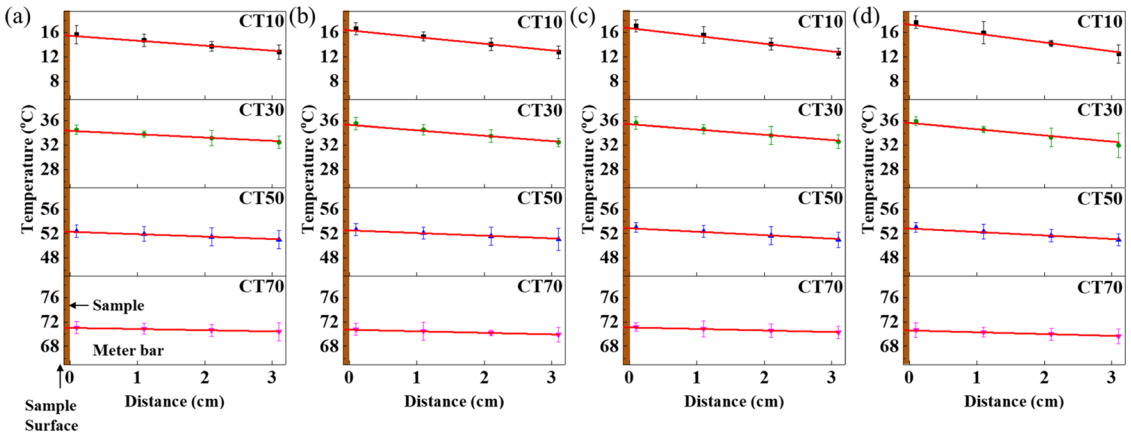

Figure 4. Temperature profile in the meter bar during the condensation test for (a) copper substrate and hydrophobic copper surface electrodeposited for (b) 10 (ED10), (c) 20 (ED20), and (d) 30 (ED30) min with a coolant temperature of 10 (CT10), 30 (CT30), 50 (CT50), and 70 (CT70) °C.

Table 1. Measured and Estimated Data from the Condensation Heat Transfer Test for the Copper Substrate (CP) and Hydrophobic Copper Surface Electrodeposited for 10 (ED10), 20 (ED20), and 30 (ED30) min

coolant temp	10 °C				30 °C				50 °C				70 °C			
sample	CP	ED10	ED20	ED30	CP	ED10	ED20	ED30	CP	ED10	ED20	ED30	CP	ED10	ED20	ED30
temp gradient (°C/cm)	−0.97	−1.30	−1.47	−1.73	−0.67	−0.93	−1.03	−1.31	−0.47	−0.53	−0.68	−0.73	−0.23	−0.30	−0.30	−0.35
surface temp (°C)	15.9 ± 1.0	16.9 ± 0.9	17.3 ± 1.0	18.0 ± 0.9	34.6 ± 0.8	35.8 ± 1.1	35.9 ± 1.1	36.2 ± 0.8	52.5 ± 1.0	52.8 ± 1.1	53.2 ± 0.9	53.3 ± 0.7	71.1 ± 1.0	70.9 ± 1.0	71.2 ± 0.8	70.8 ± 1.2

4.2, and 168.4 ± 3.7° for 10, 20, and 30 min of copper electrodeposition, respectively. The contact line of the three-phase interface (solid/air/liquid) also affects the adhesion between the two phases (water and solid surface); thus, the mobility of water droplets is enhanced on a rough hydrophobic surface.[44,45] Therefore, the contact angle hysteresis decreases with an increase in the average roughness, such as 18.9 ± 1.4, 6.3 ± 3.1, and 2.3 ± 0.8° for 10, 20, and 30 min of copper electrodeposition, respectively. In particular, the surface fabricated by 30 min of copper electrodeposition and its Teflon coating exhibited superhydrophobicity with extremely low wettability and high mobility of water droplets. These results suggest that superhydrophobicity can be realized on copper using electrodeposition without surface oxidation of copper-forming nanoneedle-structured CuO, which is generally used to fabricate superhydrophobic surfaces on copper.[29,46]

3.2. Condensation Heat Transfer. The condensation heat transfer of four types of samples (CS, ED10, ED20, and ED30) was tested using the setup shown in Figure 1 with changing coolant temperature. The coolant temperature controlled the temperature of the surface, and the condition of the chamber was maintained at 90 °C with hot water at the bottom. We measured the stabilized temperature of each location in the meter bar (Figure 1), and Figure 4 shows the temperature profile in the meter bar. The temperature gradient (slope of temperature vs. distance in Figure 4) was estimated by linear fitting and is summarized in Table 1.[47] The sample surface temperature was calculated considering the linear relationship between the temperature and location in the meter bar (Table 1). Even though the thermal conductivity of Teflon (poly(tetrafluoroethylene)) is 0.25 W/m·K, which is relatively very lower than that of copper, the Teflon layer shows negligible thermal resistance on the copper surface, due to its extremely low thickness (~2 nm).[48] The sample surface had a lower temperature with a decrease in the coolant temperature; thus, the temperature difference between the vapor and sample surface increases, thereby enhancing water condensation. In addition, the decrease in the coolant temperature contributed to an increase in the temperature gradient in the meter bar. When the coolant temperature was 70 °C, the temperature gradients were −0.23, −0.30, −0.30, and −0.35 for CS, ED10, ED20, and ED30, respectively, showing no significant difference. However, the hydrophobic surface with improved mobility (low contact angle hysteresis) of the water droplet shows a significantly enhanced temperature gradient with a decrease in the coolant temperature. In particular, the temperature gradient of ED30 was higher than that of CS by approximately 1.78-fold at a coolant temperature of 10 °C, while ED30 shows approximately 1.55-fold higher temperature gradient than that of CS at a coolant temperature of 50 °C. Hydrophobized copper electrodeposition with high mobility of water droplets also increases the surface temperature (Table 1) for coolant temperatures below 50 °C. In contrast, no significant difference was observed in the surface temperature at a coolant temperature of 70 °C.

The increased temperature gradient in the meter bar and surface temperature of the sample due to the enhanced dewetting and mobility of water droplets on the hydrophobized copper electrodeposition indicates a change in the heat transfer in the copper meter bar. The transferred heat (Q) from the sample surface to the coolant through the meter bar can be calculated using the following equation[49,50]

$$Q = \lambda \cdot \Delta T / d \quad (1)$$

where λ, ΔT, and d are the thermal conductivity of the copper meter bar (391.1 W/(m·K)), temperature difference, and distance between thermocouples, respectively.[17] The temperature gradient summarized in Table 1 corresponds to $\Delta T/d$;

https://doi.org/10.1021/acsomega.2c02522
ACS Omega 2022, 7, 19021−19029

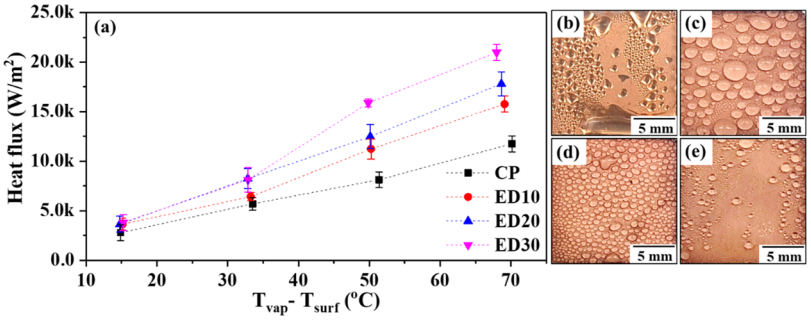

Figure 5. Condensation heat transfer; (a) estimated heat flux and appearance of condensed water on (b) copper substrate and hydrophobic copper surface electrodeposited for (c) 10 (ED10), (d) 20 (ED20), and (e) 30 (ED30) min.

thus, the heat flux through the copper meter bar can be calculated.[51,52] Figure 5 shows the calculated heat flux (condensation heat transfer) as a function of the temperature difference between the water vapor and the sample surface. The surface appearances of the sample with condensed water droplets are shown in Figure 5.

A lower temperature of the sample surface than that of water vapor causes the condensation of water on the surface. Thus, the latent heat of condensation is released on the surface, which is transferred to the meter bar and then to the coolant to condense more water on the sample surface, producing a greater heat flux with a higher temperature gradient in the meter bar. In addition, the higher the latent heat by condensation, the higher the surface temperature of the sample. For the coolant temperature of 70 °C, because the temperature gradients of the samples did not show any significant difference, the heat flux by condensation heat transfer showed a similar value for each sample. However, with a decrease in the coolant temperature from 70 to 10 °C, the heat flux on the CS increases by more than 4.2-fold. Nevertheless, the hydrophobized copper-electrodeposited surfaces (ED10, ED20, and ED30) showed a more significant increase in heat flux than for the CS. The decrease in the coolant temperature from 70 to 10 °C increases the condensation heat flux by more than 4.3-, 4.9-, and 5.5-fold for ED10, ED20, and ED30, respectively. In particular, ED30 with the lowest contact angle hysteresis showed the most significant increase in the heat flux with the highest surface temperature. Therefore, the temperature difference between the water vapor and sample surface ($T_{vap} - T_{surf}$) slightly decreases with the condensation heat transfer.

The shape and mobility of water droplets on a superhydrophobic copper surface enhance the condensation heat transfer. The CS surface, easily wettable by water, shows widespread water droplets (Figure 5b) as a filmwise condensation. Moreover, the water droplet is almost immobile on the CS surface, and the water film wetting the copper surface is not easily removed by gravity. However, the condensed water shows a spherical shape on the hydrophobic copper surfaces (Figure 5c−e), indicating dropwise condensation due to their dewetting property, which shows a high apparent contact angle of the water droplet. Despite the spherical shape of the condensed water droplets, the hydrophobic surfaces demonstrate different sizes of water droplets. ED10 showed the largest number of water droplets pinned on the surface. The size of the water droplets was smaller on the ED20 surface than in the case of ED10. The gravity of a water droplet on a vertically inclined hydrophobic surface provides a force to roll off the droplet along the surface so that a small droplet is easily mobile on the surface with high mobility of water droplets (low contact angle hysteresis).[53,54] Therefore, the condensed water droplet on the ED20 surface with a lower contact angle hysteresis than that of ED10 cannot be grown up to the droplet size on the ED10 surface. In the case of ED30 with the lowest contact angle hysteresis, a significant area of noncondensed copper surface is exposed to ambient and smaller condensed water droplets than in the case of ED20. These results are attributed to the frequent roll-off of the condensed water droplet with a small size. A rolling condensed water droplet combines with other droplets along the rolling path; thus, a larger area of the cold copper surface can be exposed to humid conditions to initiate the nucleation of water condensation. These results indicate that coating with a thin hydrophobic material and controlling the surface morphology enhance water mobility, significantly improving the condensation heat transfer.

To examine the stability of the Teflon layer, the contact angle of water droplets on ED30 is measured after testing condensation heat transfer up to 7 days (Figure 6a) and

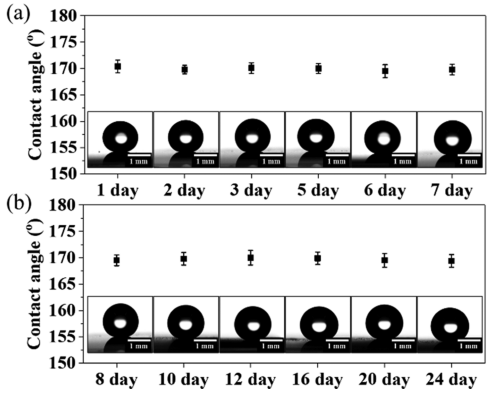

Figure 6. Contact angle of water droplets on the ED30 surface after (a) condensation heat transfer test up to 7 days and (b) exposure to air up to 24 days.

exposing to air up to 24 days (Figure 6b). During the condensation heat transfer testing, the contact angle of the water droplet on ED30 is consistently maintained at 170−175°, showing the superhydrophobicity. Moreover, the exposure of ED30 to air for a month does not affect the contact angle of 170−175°. These results indicate that the Teflon coating on roughly electrodeposited copper stably shows superhydrophobicity both under humid and air conditions over time.

https://doi.org/10.1021/acsomega.2c02522
ACS Omega 2022, 7, 19021−19029

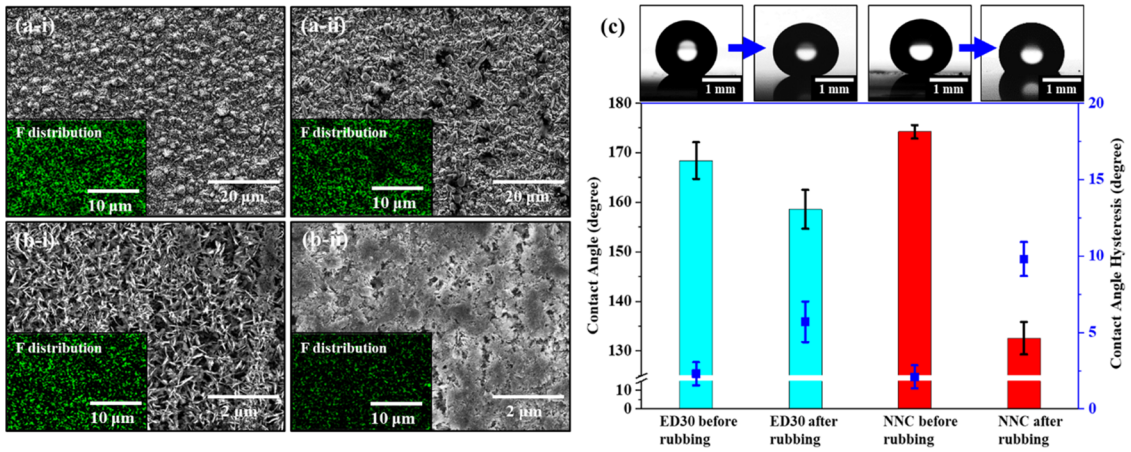

Figure 7. Surface morphology of (a) hydrophobic copper surface electrodeposited for 30 min (ED30) and (b) hydrophobic nanoneedle copper oxide surface (i) before and (ii) after rubbing. (c) Averaged static contact angle and contact angle hysteresis.

Table 2. Measured and Estimated Data from the Condensation Heat Transfer Test for the Hydrophobic Copper Surface Electrodeposited for 30 min (ED30) and Hydrophobic Nanoneedle Copper Oxide (NNC) with and without Surface Rubbing

coolant temp	10 °C				30 °C				50 °C				70 °C			
	ED30		NNC		ED30		NNC		ED30		NNC		ED30		NNC	
sample	intact	damage	intact	damage	intact	damage	intact	damage	intact	damage	intact	damage	intact	damage	intact	damage
temp gradient (°C/cm)	−1.73	−1.57	−1.87	−1.03	−1.31	−1.2	−1.49	−0.93	−0.67	−0.66	−0.8	−0.5	−0.35	−0.32	−0.4	−0.26
surface temp (°C)	18.0 ± 0.9	16.9 ± 1.0	18.3 ± 0.7	15.7 ± 1.0	36.2 ± 0.8	35.5 ± 1.3	37.3 ± 0.3	35.3 ± 0.9	53.1 ± 0.7	52.8 ± 1.1	53.7 ± 0.5	52.1 ± 1.0	70.8 ± 1.2	70.9 ± 1.1	71.7 ± 0.6	70.6 ± 1.3

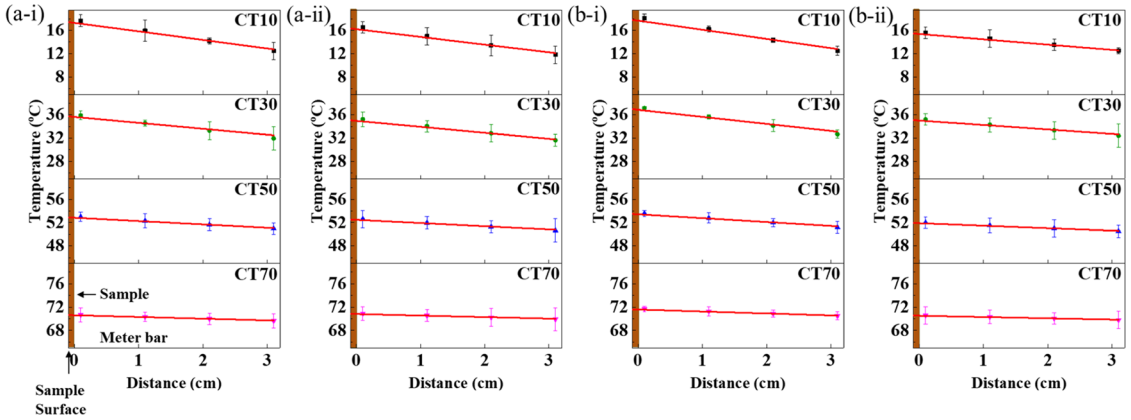

Figure 8. Temperature profile in the meter bar during the condensation test for (a) hydrophobic copper surface electrodeposited for 30 min and (b) hydrophobic nanoneedle copper oxide surface (i) before and (ii) after rubbing at a coolant temperature of 10 (CT10), 30 (CT30), 50 (CT50), and 70 (CT70) °C.

3.3. Tolerance to Physical Damage. Nanoneedle CuO (NNC) structures are generally used to fabricate superhydrophobic surfaces on copper substrates. Moreover, the enhancement of condensation heat transfer is achieved owing to its exceptional water droplet mobility. We compared the condensation heat transfer of the superhydrophobic copper-deposited surface with that of the NNC surface. In addition, the tolerance of the superhydrophobic copper-electrodeposited and NNC surfaces to mechanical damage was evaluated using a rubbing test (DIN EN ISO 11640) with an elastomer. The changes in the surface morphology, distribution of fluorine, and wettability by the rubbing test are shown in Figure 7. In the case of the superhydrophobic electrodeposited copper surface, the rough-structured surface is stronger than the elastomer; thus, no significant damage is found on the surface, and only worn elastomer particles adhere to the rough structure. Moreover, no significant change in fluorine distribution indicating the coated Teflon on the surface is observed. Such elastomer particles adhered to the rough structure inhibit the dewetting of the hydrophobic surface, so the apparent contact angle of ED30 decreases from 168.4 ± 3.7 to 158.6 ± 3.9°, indicating that the surface is still superhydrophobic. The superhydrophobic NNC surface showed a significant change in the surface structure and wettability by the rubbing test. Owing to the brittle nature of CuO, most of the sharp nanoneedle structure, which effectively supports the

https://doi.org/10.1021/acsomega.2c02522
ACS Omega 2022, 7, 19021−19029

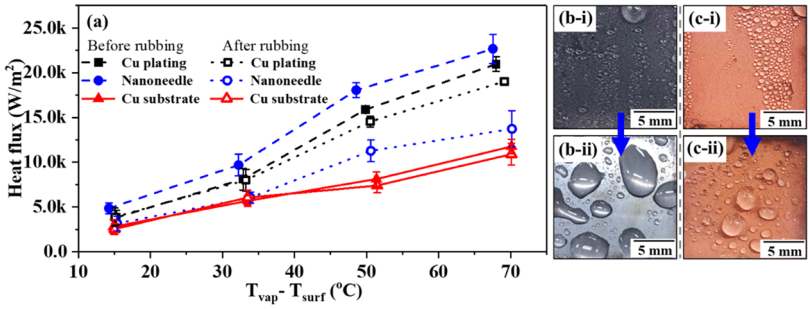

Figure 9. Condensation heat transfer of the damaged surface; (a) estimated heat flux and appearance of condensed water on (b) hydrophobic copper surface electrodeposited for 30 min and (c) hydrophobic nanoneedle copper oxide surface (i) before and (ii) after rubbing.

Cassie−Baxter interface for superhydrophobicity, is destroyed by rubbing, so the distribution of fluorine is significantly decreased, indicating the removal of the coated Teflon layer. For these reasons, the apparent contact angle of the water droplet on the damaged NNC surface is significantly decreased from 174.2 ± 1.4 to 132.6 ± 3.3°. These results imply that a simple physical contact can easily degrade the superhydrophobicity of the NNC-structured surfaces.

The degradation of hydrophobicity by damage to the micro/nanostructure can also deteriorate the condensation heat transfer; thus, we measured the condensation heat transfer of the superhydrophobic ED30 and NNC surfaces with and without the rubbing test (Figure 9). The temperature gradients and surface temperatures are summarized in Table 2. The intact NNC demonstrated higher temperature gradients (slope of temperature vs. distance in Figure 8) and surface temperature than those of ED30 for each coolant temperature, indicating better condensation heat transfer of the NNC surface than that of the ED30 surface. These results are in good agreement with the NNC surface, showing better mobility and dewetting of water droplets than those of the ED30 surface (Figure 7). Despite such superior hydrophobicity and condensation heat transfer, the damaged NNC showed significantly reduced temperature gradients by more than 35% than the entire surface because the physical damage to NNC by rubbing with an elastomer significantly deteriorates the dewetting and mobility of water droplets. However, regardless of the physical damage, the ED30 surface showed a less-significant reduction in the temperature gradient by less than 10% compared to that of the entire surface. Moreover, the temperature gradients of the damaged ED30 were higher than those of the NNC with damages for each coolant temperature.

Figure 9 illustrates the condensation heat transfer calculated from the temperature gradients in Table 2 and the surface appearance during condensation. In the case of the NNC surface, the condensation heat transfer values are 4.8 ± 0.6, 9.7 ± 1.2, 18.1 ± 0.8, and 2.3 ± 1.6 (kW/m^2) for the coolant temperatures of 10, 30, 50, and 70 °C, respectively, which are higher than those of the ED30 surface by less than 15%. In addition, the temperature difference between the humid atmosphere and the sample surface of NNC is lower than that of the ED30 surface. These results indicate that the superhydrophobic NNC has superior condensation heat transfer compared to that of the superhydrophobic electrodeposited copper surface. Nevertheless, a physical rubbing test destroying the brittle nanoneedle CuO structure diminishes the dewetting and mobility of water droplets; thus, the size of the condensed water droplet pinned on the surface significantly increases (Figure 9b). Such changes in the wetting of the condensed water decrease the condensation heat transfer by more than 35%. Although the condensation heat transfer of the entire ED30 surface is slightly lower than that of the entire NNC surface, the dewetting and mobility of water droplets on the damaged ED30 surface are better than those on the NNC surface. Therefore, smaller condensed water droplets were pinned on the damaged ED30 surface (Figure 9c) than on the damaged NNC surface (Figure 9b). These results indicate that the superhydrophobic surface fabricated on an electrodeposited copper surface has superior physical contact tolerance compared to that of the superhydrophobic surface with a nanoneedle CuO structure. Owing to the robustness of the rough structure by copper electrodeposition, a stable surface with dewetting and mobility of water droplets can be enabled against physical contacts, which may destroy the rough surface structure of NNC, supporting the superhydrophobicity. Therefore, the condensation heat transfer values of the damaged ED30 surface are higher than those of the damaged NNC surface by more than 22%, such as 3.9 ± 1.0, 8.0 ± 1.2, 14.5 ± 0.6, and 19.0 ± 0.4 (kW/m^2) for the coolant temperatures of 10, 30, 50, and 70 °C, respectively. Stable performance against unwanted physical contacts and physical robustness of the surface structure are two of the most important characteristics for the practical application of hydrophobic surfaces. Therefore, although the hydrophobic performance was slightly less than that of the previous nanoneedle CuO structure, the physically robust rough structure by copper electrodeposition can be a potential candidate for practical applications of hydrophobic surfaces, including condensation heat transfer. Moreover, since hydrophilic or hydrophilic/hydrophobic hybrid surfaces provide benefits in boiling heat transfer, the application of a durable rough electrodeposited copper surface with scalability and practical feasibility can be extended to heat exchange using boiling heat transfer.[55−60]

4. CONCLUSIONS

A multifunctional superhydrophobic surface can be fabricated using a thin Teflon coating on an electrodeposited copper surface. The microscale roughness of the copper deposit increases with an increase in the electrodeposition duration, thereby enhancing the dewetting and mobility of the water droplet. This enhancement contributes to the easy roll-off of condensed water droplets on the cold surface; thus, the surface of an electrodeposited copper layer with a Teflon coating shows a significant improvement in the condensation heat transfer. Moreover, the rough microscale structure fabricated by copper electrodeposition has a better tolerance against physical contacts that destroy the rough surface structure, such

https://doi.org/10.1021/acsomega.2c02522
ACS Omega 2022, 7, 19021−19029

as rubbing, compared to that of the nanoneedle CuO structure, which is generally used to fabricate superhydrophobic surfaces on copper. Therefore, the superhydrophobic electrodeposited copper surface shows stable condensation heat transfer. In contrast, the superhydrophobic nanoneedle CuO surface is significantly damaged by surface rubbing, which causes significant debilitation in condensation heat transfer.

AUTHOR INFORMATION

Corresponding Authors

Junghoon Lee − *Department of Metallurgical Engineering, Pukyong National University, Busan 48513, Republic of Korea;* orcid.org/0000-0002-7740-1633; Phone: +82-51-629-6345; Email: jlee1@pknu.ac.kr; Fax: +82-51-629-6339

Wonsub Chung − *Department of Materials Science and Engineering, Pusan National University, Busan 46241, Republic of Korea*; Phone: +82-51-510-2386; Email: wschung1@pusan.ac.kr; Fax: +82-51-510-4457

Authors

Junghyun Park − *Department of Materials Science and Engineering, Pusan National University, Busan 46241, Republic of Korea; Korea Institute of Ceramic Engineering and Technology, Jinju, Gyeongsangnam-do 52851, Republic of Korea*

Donghyun Kim − *Korea Institute of Ceramic Engineering and Technology, Jinju, Gyeongsangnam-do 52851, Republic of Korea*

Hyunsik Kim − *Korea Institute of Ceramic Engineering and Technology, Jinju, Gyeongsangnam-do 52851, Republic of Korea*

Woon Ik Park − *Department of Materials Science and Engineering, Pukyoung National University, Busan 48513, Republic of Korea*

Complete contact information is available at: https://pubs.acs.org/10.1021/acsomega.2c02522

Notes

The authors declare no competing financial interest.

ACKNOWLEDGMENTS

J.L. acknowledges the support from the local industry promotion business linked with public institutions (Gyeongnam, P0004798) funded by the Ministry of Trade, Industry and Energy (MOTIE, Korea).

REFERENCES

(1) Parker, A. R.; Lawrence, C. R. Water capture by a desert beetle. *Nature* **2001**, *414*, 33−34.

(2) Peters, T. B.; McCarthy, M.; Allison, J.; Dominguez-Espinosa, F. A.; Jenicek, D.; Kariya, H. A.; Staats, W. L.; Brisson, J. G.; Lang, J. H.; Wang, E. N. Design of an integrated loop heat pipe air-cooled heat exchanger for high performance electronics. *IEEE Trans. Compon., Packag., Manuf. Technol.* **2012**, *2*, 1637−1648.

(3) Humplik, T.; Lee, J.; O'Hern, S. C.; O'hern, S.; Fellman, B.; Baig, M.; Hassan, S.; Atieh, M.; Rahman, F.; Laoui, T.; Karnik, R. Nanostructured materials for water desalination. *Nanotechnology* **2011**, *22*, No. 292001.

(4) Preston, D. J.; Lu, Z.; Song, Y.; Zhao, Y.; Wilke, K. L.; Antao, D. S.; Louis, M.; Wang, E. N. Heat transfer enhancement during water and hydrocarbon condensation on lubricant infused surfaces. *Sci. Rep.* **2018**, *8*, No. 540.

(5) Peng, B.; Ma, X.; Lan, Z.; Xu, W.; Wen, R. Experimental investigation on steam condensation heat transfer enhancement with vertically patterned hydrophobic−hydrophilic hybrid surfaces. *Int. J. Heat Mass Transfer* **2015**, *83*, 27−38.

(6) Oh, J.; Zhang, R.; Shetty, P. P.; Krogstad, J. A.; Braun, P. V.; Miljkovic, N. Thin film condensation on nanostructured surfaces. *Adv. Funct. Mater.* **2018**, *28*, No. 1707000.

(7) Niu, D.; Tang, G. The effect of surface wettability on water vapor condensation in nanoscale. *Sci. Rep.* **2016**, *6*, No. 19192.

(8) Ho, J.; Leong, K. Effect of fin pitch on the filmwise condensation of steam on three-dimensional conical pin fin arrays: A comparative study. *Int. J. Heat Mass Transfer* **2020**, *150*, No. 119328.

(9) Starostin, A.; Valtsifer, V.; Barkay, Z.; Legchenkova, I.; Danchuk, V.; Bormashenko, E. Drop-wise and film-wise water condensation processes occurring on metallic micro-scaled surfaces. *Appl. Surf. Sci.* **2018**, *444*, 604−609.

(10) Miljkovic, N.; Enright, R.; Nam, Y.; Lopez, K.; Dou, N.; Sack, J.; Wang, E. N. Jumping-droplet-enhanced condensation on scalable superhydrophobic nanostructured surfaces. *Nano Lett.* **2013**, *13*, 179−187.

(11) Wang, G.; Liu, S.; Wei, S.; Liu, Y.; Lian, J.; Jiang, Q. Robust superhydrophobic surface on Al substrate with durability, corrosion resistance and ice-phobicity. *Sci. Rep.* **2016**, *6*, No. 20933.

(12) Seo, D.; Lee, C.; Nam, Y. Influence of geometric patterns of microstructured superhydrophobic surfaces on water-harvesting performance via dewing. *Langmuir* **2014**, *30*, 15468−15476.

(13) Ahlers, M.; Buck-Emden, A.; Bart, H.-J. Is dropwise condensation feasible? A review on surface modifications for continuous dropwise condensation and a profitability analysis. *J. Adv. Res.* **2019**, *16*, 1−13.

(14) Kim, S.; Kim, K. J. Dropwise condensation modeling suitable for superhydrophobic surfaces. *J. Heat Transfer* **2011**, *133*, No. 081502.

(15) Miljkovic, N.; Enright, R.; Wang, E. N. Effect of droplet morphology on growth dynamics and heat transfer during condensation on superhydrophobic nanostructured surfaces. *ACS Nano* **2012**, *6*, 1776−1785.

(16) Rose, J. W. Dropwise condensation theory and experiment: a review. *Proc. Inst. Mech. Eng., Part A* **2002**, *216*, 115−128.

(17) Nath, P.; Chopra, K. Thermal conductivity of copper films. *Thin Solid Films* **1974**, *20*, 53−62.

(18) Uher, C. Thermal Conductivity of Metals. In *Thermal Conductivity*; Springer, 2004; pp 21−91.

(19) Qu, X.-h.; Zhang, L.; Mao, W.; Ren, S.-b. Review of metal matrix composites with high thermal conductivity for thermal management applications. *Prog. Nat. Sci.* **2011**, *21*, 189−197.

(20) Enright, R.; Miljkovic, N.; Al-Obeidi, A.; Thompson, C. V.; Wang, E. N. Condensation on superhydrophobic surfaces: the role of local energy barriers and structure length scale. *Langmuir* **2012**, *28*, 14424−14432.

(21) Ou, J.; Hu, W.; Liu, S.; Xue, M.; Wang, F.; Li, W. Superoleophobic textured copper surfaces fabricated by chemical etching/oxidation and surface fluorination. *ACS Appl. Mater. Interfaces* **2013**, *5*, 10035−10041.

(22) Enright, R.; Miljkovic, N.; Dou, N.; Nam, Y.; Wang, E. N. Condensation on superhydrophobic copper oxide nanostructures. *J. Heat Transfer* **2013**, *135*, No. 091304.

(23) Zhang, Y.; Feyerabend, F.; Tang, S.; Hu, J.; Lu, X.; Blawert, C.; Lin, T. A study of degradation resistance and cytocompatibility of super-hydrophobic coating on magnesium. *Mater. Sci. Eng., C* **2017**, *78*, 405−412.

(24) Erbil, H. Y.; Cansoy, C. E. Range of applicability of the Wenzel and Cassie− Baxter equations for superhydrophobic surfaces. *Langmuir* **2009**, *25*, 14135−14145.

(25) Kim, H.; Nam, Y. Condensation Heat Transfer Performance of Nano-Engineered Cu Surfaces. In *Journal of Physics: Conference Series*; IOP Publishing, 2014; p 012109.

(26) Wilke, K. L.; Preston, D. J.; Lu, Z.; Wang, E. N. Toward condensation-resistant omniphobic surfaces. *ACS Nano* **2018**, *12*, 11013−11021.
(27) Miura, S.; Honma, H. Advanced copper electroplating for application of electronics. *Surf. Coat. Technol.* **2003**, *169*−*170*, 91−95.
(28) Torresin, D.; Tiwari, M. K.; Del Col, D.; Poulikakos, D. Flow condensation on copper-based nanotextured superhydrophobic surfaces. *Langmuir* **2013**, *29*, 840−848.
(29) Kim, H.; Nam, Y. Condensation behaviors and resulting heat transfer performance of nano-engineered copper surfaces. *Int. J. Heat Mass Transfer* **2016**, *93*, 286−292.
(30) Nam, Y.; Ju, Y. S. A comparative study of the morphology and wetting characteristics of micro/nanostructured Cu surfaces for phase change heat transfer applications. *J. Adhes. Sci. Technol.* **2013**, *27*, 2163−2176.
(31) Haghdoost, A.; Pitchumani, R. Fabricating superhydrophobic surfaces via a two-step electrodeposition technique. *Langmuir* **2014**, *30*, 4183−4191.
(32) Jain, R.; Pitchumani, R. Facile fabrication of durable copper-based superhydrophobic surfaces via electrodeposition. *Langmuir* **2018**, *34*, 3159−3169.
(33) Kuang, Y.; Jiang, F.; Zhu, T.; Wu, H.; Yang, X.; Li, S.; Hu, C. One-step electrodeposition of superhydrophobic copper coating from ionic liquid. *Mater. Lett.* **2021**, *303*, No. 130579.
(34) Boland, J.; Chao, Y.-H.; Suzuki, Y.; Tai, Y. In *Micro Electret Power Generator*, The Sixteenth Annual International Conference on Micro Electro Mechanical Systems, MEMS-03 Kyoto; IEEE, Kyoto, 2003; pp 538−541.
(35) Yang, M. K.; French, R. H.; Tokarsky, E. W. Optical properties of Teflon AF amorphous fluoropolymers. *J. Micro/Nanolithogr., MEMS, MOEMS* **2008**, *7*, No. 033010.
(36) Wang, R.; Wu, F.; Xing, D.; Yu, F.; Gao, X. Density maximization of one-step electrodeposited copper nanocones and dropwise condensation heat-transfer performance evaluation. *ACS Appl. Mater. Interfaces* **2020**, *12*, 24512−24520.
(37) Cho, H. J.; Sresht, V.; Wang, E. N. Predicting surface tensions of surfactant solutions from statistical mechanics. *Langmuir* **2018**, *34*, 2386−2395.
(38) Gao, X.; Yao, X.; Jiang, L. Effects of rugged nanoprotrusions on the surface hydrophobicity and water adhesion of anisotropic micropatterns. *Langmuir* **2007**, *23*, 4886−4891.
(39) Xiu, Y.; Zhu, L.; Hess, D. W.; Wong, C. Hierarchical silicon etched structures for controlled hydrophobicity/superhydrophobicity. *Nano Lett.* **2007**, *7*, 3388−3393.
(40) Tantavichet, N.; Pritzker, M. Copper electrodeposition in sulphate solutions in the presence of benzotriazole. *J. Appl. Electrochem.* **2006**, *36*, 49−61.
(41) Ruythooren, W.; Attenborough, K.; Beerten, S.; Merken, P.; Fransaer, J.; Beyne, E.; Van Hoof, C.; De Boeck, J.; Celis, J.-P. Electrodeposition for the synthesis of microsystems. *J. Micromech. Microeng.* **2000**, *10*, No. 101.
(42) Boreyko, J. B.; Baker, C. H.; Poley, C. R.; Chen, C.-H. Wetting and dewetting transitions on hierarchical superhydrophobic surfaces. *Langmuir* **2011**, *27*, 7502−7509.
(43) Sheng, Y.-J.; Jiang, S.; Tsao, H.-K. Effects of geometrical characteristics of surface roughness on droplet wetting. *J. Chem. Phys.* **2007**, *127*, No. 234704.
(44) Wang, D.; Jiang, Y.; Zhu, Z.; Yin, W.; Asawa, K.; Choi, C.-H.; Drelich, J. W. Contact line and adhesion force of droplets on concentric ring-textured hydrophobic surfaces. *Langmuir* **2020**, *36*, 2622−2628.
(45) Ding, Y.; Jia, L.; Peng, Q.; Guo, J. Critical sliding angle of water droplet on parallel hydrophobic grooved surface. *Colloids Surf., A* **2020**, *585*, No. 124083.
(46) Xiao, F.; Yuan, S.; Liang, B.; Li, G.; Pehkonen, S. O.; Zhang, T. Superhydrophobic CuO nanoneedle-covered copper surfaces for anticorrosion. *J. Mater. Chem. A* **2015**, *3*, 4374−4388.
(47) Ryu, S.; Han, J.; Kim, J.; Lee, C.; Nam, Y. Enhanced heat transfer using metal foam liquid supply layers for micro heat spreaders. *Int. J. Heat Mass Transfer* **2017**, *108*, 2338−2345.
(48) Lee, J.; Shin, S.; Jiang, Y.; Jeong, C.; Stone, H. A.; Choi, C. H. Oil-impregnated nanoporous oxide layer for corrosion protection with self-healing. *Adv. Funct. Mater.* **2017**, *27*, No. 1606040.
(49) Makkonen, L. Young's equation revisited. *J. Phys.: Condens. Matter.* **2016**, *28*, No. 135001.
(50) Adam, N. K. Use of the term 'Young's Equation'for contact angles. *Nature* **1957**, *180*, 809−810.
(51) Shi, J.; Zheng, G.; Chen, Z.; Dang, C. Experimental study of flow condensation heat transfer in tubes partially filled with hydrophobic annular metal foam. *Int. J. Heat Mass Transfer* **2019**, *136*, 1265−1272.
(52) Yi, Q.; Tian, M.; Yan, W.; Qu, X.; Chen, X. Visualization study of the influence of non-condensable gas on steam condensation heat transfer. *Appl. Therm. Eng.* **2016**, *106*, 13−21.
(53) Gao, L.; McCarthy, T. J. Contact angle hysteresis explained. *Langmuir* **2006**, *22*, 6234−6237.
(54) Zhang, L.; Xu, Z.; Lu, Z.; Du, J.; Wang, E. N. Size distribution theory for jumping-droplet condensation. *Appl. Phys. Lett.* **2019**, *114*, No. 163701.
(55) Chen, R.; Lu, M.-C.; Srinivasan, V.; Wang, Z.; Cho, H. H.; Majumdar, A. Nanowires for enhanced boiling heat transfer. *Nano Lett.* **2009**, *9*, 548−553.
(56) Yao, Z.; Lu, Y.-W.; Kandlikar, S. G. Direct growth of copper nanowires on a substrate for boiling applications. *Micro Nano Lett.* **2011**, *6*, 563−566.
(57) Shin, S.; Kim, B. S.; Choi, G.; Lee, H.; Cho, H. H. hybrid structure by electrodeposition for efficient boiling heat transfer. *Appl. Phys. Lett.* **2012**, *101*, No. 251909.
(58) Shin, H. K.; Park, M.; Kim, H.-Y.; Park, S.-J. Thermal property and latent heat energy storage behavior of sodium acetate trihydrate composites containing expanded graphite and carboxymethyl cellulose for phase change materials. *Appl. Therm. Eng.* **2015**, *75*, 978−983.
(59) Wen, R.; Li, Q.; Wang, W.; Latour, B.; Li, C. H.; Li, C.; Lee, Y.-C.; Yang, R. Enhanced bubble nucleation and liquid rewetting for highly efficient boiling heat transfer on two-level hierarchical surfaces with patterned copper nanowire arrays. *Nano Energy* **2017**, *38*, 59−65.
(60) Udaya Kumar, G.; Suresh, S.; Thansekhar, M.; Halpati, D. Role of inter-nanowire distance in metal nanowires on pool boiling heat transfer characteristics. *J. Colloid Interface. Sci.* **2018**, *532*, 218−230.

https://doi.org/10.1021/acsomega.2c02522
ACS Omega 2022, 7, 19021−19029